Inorganic Chemistry

including bioinorganic chemistry

September 16, 2013
Volume 52, Number 18
pubs.acs.org/IC

Nonlinear Optical Behavior in Crystals of Lead Borates

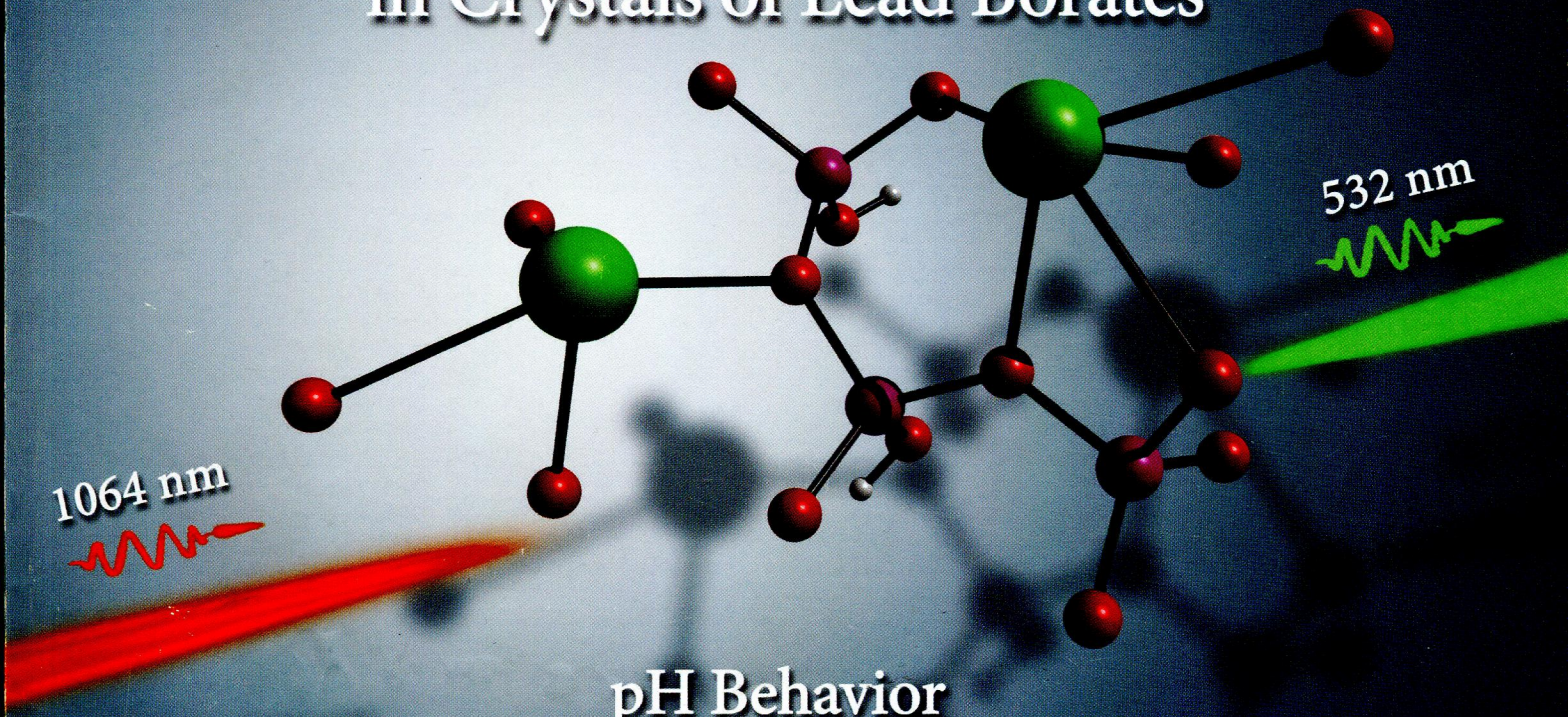

pH Behavior

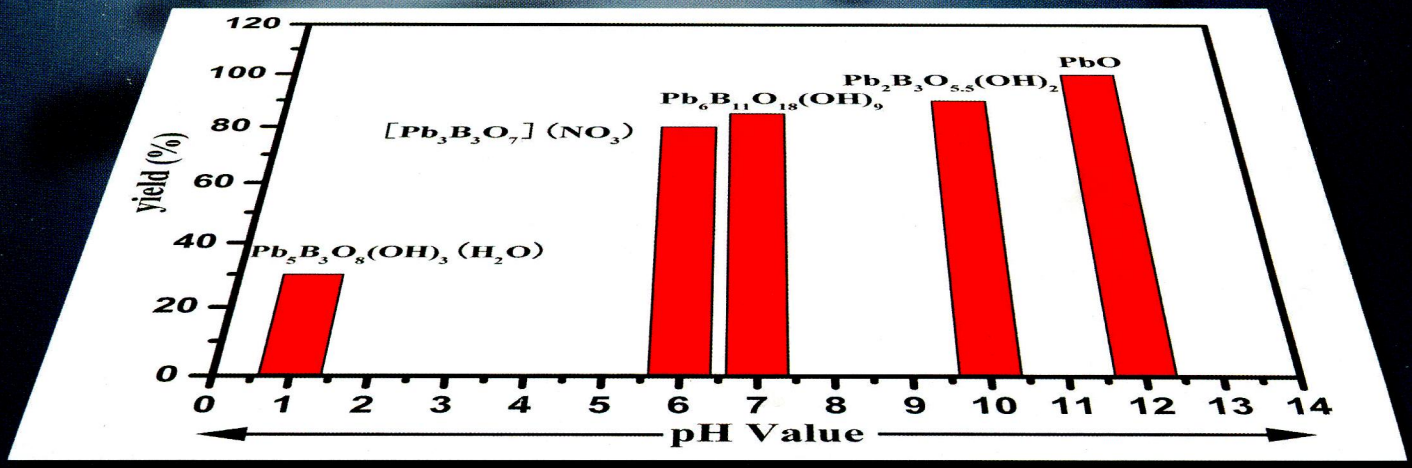

Inorganic Chemistry

SEPTEMBER 16, 2013
VOLUME 52 ISSUE 18

INOCAJ 52(18) 10217–10704 (2013)
ISSN 0020-1669
Registered in the U.S. Patent and Trademark Office

ON THE COVER: By using lead(II) metaborate as the starting material, a series of lead(II) borates can be obtained by just adjusting the pH value of the reaction system. The polar species $Pb_2B_3O_{3.5}(OH)$ displays a strong second-harmonic-generation response due to the synergistic effect of the stereoactive lone-pairs on the Pb^{2+} cations. This paper was inadvertently published in a previous issue. See J.-L. Song, C.-L. Hu, X. Xu, F. Kong, and J.-G. Mao *Inorg. Chem.* **2013**, *52* (15), 8979-8086.

Communications

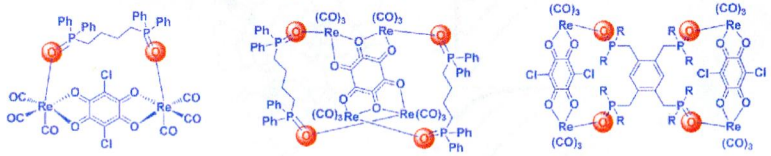

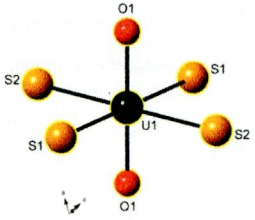

10223 S dx.doi.org/10.1021/ic401605m

Quantitative Fluorescent Detection of Pyrophosphate with Quinoline-Ligated Dinuclear Zinc Complexes

Yuji Mikata,* Anna Ugai, Risa Ohnishi, and Hideo Konno

Dinuclear zinc complex $[Zn_2(TQHPN)(AcO)]^{2+}$ exhibits characteristic fluorescence response (λ_{ex} = 317 nm and λ_{em} = 455 nm) toward pyrophosphate (PPi) with maximum fluorescence upon 1:1 Zn_2(TQHPN)–PPi complex formation. The crystallographic investigation utilizing P^1P^2–Ph_2PPi revealed that the fluorescent response mechanism of **1** is due to intramolecular excimer formation of two quinoline rings.

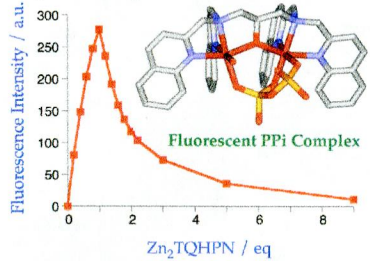

10226 S dx.doi.org/10.1021/ic401658n

Synthesis and Structural Characterization of Bis(2-oxoimidazolyl)hydroborato Complexes: A New Class of Bidentate Oxygen-Donor Ligands

Ahmed Al-Harbi, Yi Rong, and Gerard Parkin*

A new class of bidentate ligands that feature oxygen donors, namely, the bis(2-oxo-1-*tert*-butylimidazolyl)hydroborato and bis(2-oxo-1-methylbenzimidazolyl)hydroborato ligands, $[Bo^{Bu^t}]$ and $[Bo^{MeBenz}]$, have been synthesized via the reactions of MBH_4 with 2 equiv of the respective 2-imidazolone. Chelation of $[Bo^{Bu^t}]$ and $[Bo^{MeBenz}]$ to a metal center results in a flexible eight-membered ring that is capable of adopting a "boatlike" conformation that allows for secondary M···H–B interactions.

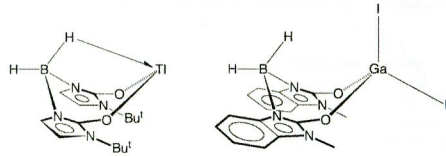

10229 S dx.doi.org/10.1021/ic401561k

Unsymmetrical Bimetallic Complexes with M^{II}–(μ-OH)–M^{III} Cores ($M^{II}M^{III}$ = $Fe^{II}Fe^{III}$, $Mn^{II}Fe^{III}$, $Mn^{II}Mn^{III}$): Structural, Magnetic, and Redox Properties

Yohei Sano, Andrew C. Weitz, Joseph W. Ziller, Michael P. Hendrich, and A. S. Borovik*

A synthetic approach has been develop for preparation of a heterobimetallic complex with a Mn^{II}–(μ-OH)–Fe^{III} core, in which the metal centers have different coordination environments. Homobimetallic complexes with Mn^{II}–(μ-OH)–Mn^{III} and Fe^{II}–(μ-OH)–Fe^{III} cores have also been isolated and serve as control species. Structural and physical data support the assignment of these complexes.

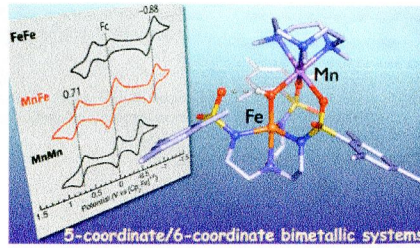

10232 S dx.doi.org/10.1021/ic401722c

Hybrid Inorganic–Organic Polyrotaxane, Pseudorotaxane, and Sandwich

Li Yu, Mian Li, Xiao-Ping Zhou, and Dan Li*

Inorganic–organic hybrid adducts, including polyrotaxane, pseudorotaxane, and sandwich, are synthesized from solvothermal reactons of copper(I)/silver(I) halide/pseudohalide and cyclobis(paraquat-*p*-phenylene)/cyclobis(paraquat-4,4′-biphenylene).

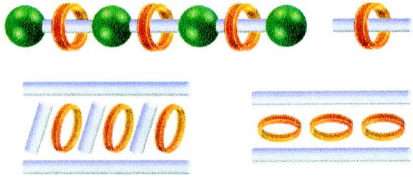

10235 S dx.doi.org/10.1021/ic4020064

Molecular Nanoscale Magnetic Refrigerants: A Ferrimagnetic $\{Cu^{II}_{15}Gd^{III}_{7}\}$ Cagelike Cluster from the Use of Pyridine-2,6-dimethanol

Despina Dermitzaki, Giulia Lorusso, Catherine P. Raptopoulou, Vassilis Psycharis, Albert Escuer,* Marco Evangelisti,* Spyros P. Perlepes,* and Theocharis C. Stamatatos*

The employment of pyridine-2,6-dimethanol in 3d/4f metal cluster chemistry has resulted in a new $\{Cu^{II}_{15}Gd^{III}_{7}\}$ cagelike molecule with a beautiful structure and an overall ferrimagnetic behavior with an appreciable ground-state spin value. The compound shows a satisfactory magnetocaloric effect with $-\Delta S_m^{max} = 22.2$ J kg^{-1} K^{-1}.

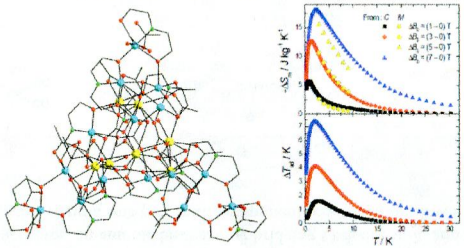

Articles

10238 S dx.doi.org/10.1021/ic302705f

Germanate with Three-Dimensional 12 × 12 × 11-Ring Channels Solved by X-ray Powder Diffraction with Charge-Flipping Algorithm

Yan Xu, Leifeng Liu, Daniel M. Chevrier, Junliang Sun,* Peng Zhang,* and Jihong Yu*

A novel germanate was hydrothermally prepared in the concentrated gel system using 1,5-bis(methylpyrrolidinium)pentane dihydroxide as the structure-directing agent. The structure was solved from synchrotron X-ray powder diffraction data using the charge-flipping algorithm combined with simulated annealing and EXAFS characterization. Its framework is built of 7-connected Ge_7 clusters and additional $GeO_3(OH)$ units forming a three-dimensional interrupted open framework with intersecting 12 × 12 × 11-ring channels.

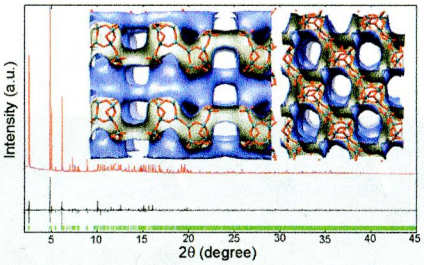

10245 S dx.doi.org/10.1021/ic302730v

Electrochemical Evidence of Intramolecular Electronic Communication in Zr and Hf Phthalocyanines Bearing Ferrocene-Containing β-Diketonato Axial Ligands: Structure of [PcHf(FcCOCHCOC$_6$H$_5$)$_2$]

Blenerhassitt E. Buitendach, Anna Gągor, and Jannie C. Swarts*

Zirconium(IV) and hafnium(IV) phthalocyanine complexes bearing two axial ferrocene-containing β-diketonato ligands were synthesized and investigated structurally and electrochemically. A linear relationship between the sum of group electronegativities of each β-diketonato R group, $\Sigma\chi_R$, and the ferrocenyl oxidation potential exists.

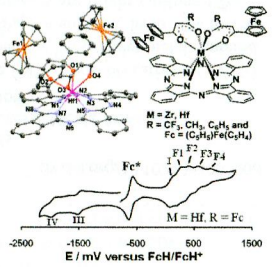

10258 S dx.doi.org/10.1021/ic4001208

Geometry and Temperature Dependence of *meso*-Aryl Rotation in Strained Metalloporphyrins: Adjustable Turnstile Molecules

Zaichun Zhou,* Xi Zhang, Qiuhua Liu,* Ziqiang Yan, Chengjin Lv, and Ge Long

The rotation of *meso*-aryl groups in porphyrins depends on the degree of macrocyclic distortion and is also influenced by the surrounding temperature.Two empirical methods are developed to acquire the rotational barrier. This type of strained molecule can act as an adjustable molecular turnstile through adjusting the degree of macrocyclic distortion and changing the surrounding temperature.

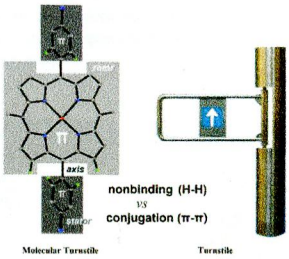

10264 S dx.doi.org/10.1021/ic400303x

Synergy in Photomagnetic/Ferromagnetic *Sub*-50 nm Core-Multishell Nanoparticles

Nada Dia, Laurent Lisnard,* Yoann Prado, Alexandre Gloter, Odile Stéphan, François Brisset, Hala Hafez, Zeinab Saad, Corine Mathonière,* Laure Catala,* and Talal Mallah

Photomagnetic/ferromagnetic *sub*-50 nm core multishell coordination nanoparticles have been synthesized with a good control over the dispersity (10% standard deviation) and targeted size at each step, using a surfactant-free procedure. Photomagnetic and magnetic studies reveal (i) a uniform reversal of the magnetization of the heterostructured nanoparticles and (ii) a persistent *increase* of the photoinduced magnetization up to the ordering temperature (60 K) of the ferromagnetic component because of the unique synergetic coupling.

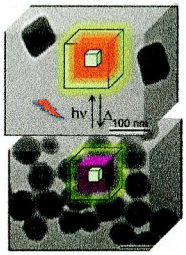

10275 S dx.doi.org/10.1021/ic400560k

Infrared Spectra of H_2ThS and H_2US in Noble Gas Matrixes: Enhanced H-An-S Covalent Bonding

Xuefeng Wang, Lester Andrews,* K. Sahan Thanthiriwatte, and David A. Dixon*

The major products of the reaction of Th and U with H_2S are H_2ThS and H_2US, and have 71−85 cm^{-1} *higher* hydrogen-actinide stretching frequencies than the oxygen analogues. The actinide-hydrogen bonding is enhanced in the actinide sulfides through back-bonding of a S 3p electron pair to a vacant 6d orbital, which is delocalized over the H atoms.

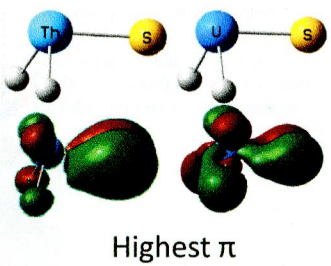

10286 S dx.doi.org/10.1021/ic400598x

Porous and Robust Lanthanide Metal-Organoboron Frameworks as Water Tolerant Lewis Acid Catalysts

Yan Liu, Ke Mo, and Yong Cui*

Porous and robust 12-connected metal–organic frameworks (MOFs) were constructed by linking tetranuclear lanthanide (Ln) clusters with organoboron-derived tricarboxylate ligands. The high-connectivity Ln-MOFs feature remarkable thermal and hydrolytic stability and a high density of isolated Lewis acid Nd(III) and B(III) sites on the pore surfaces. The Nd-MOF assisted with sodium dodecylsulfate was found to be highly effective, recyclable, and reusable solid catalyst for the carbonyl allylation reaction, the Diels–Alder reaction, and the Strecker-type reaction in water.

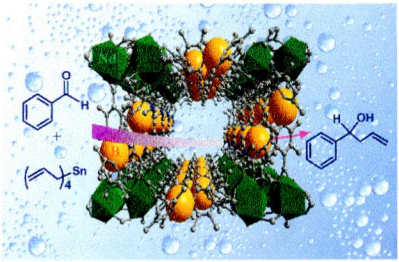

10292 S dx.doi.org/10.1021/ic400600c

Charged Bis-Cyclometalated Iridium(III) Complexes with Carbene-Based Ancillary Ligands

Filippo Monti, Florian Kessler, Manuel Delgado, Julien Frey, Federico Bazzanini, Gianluca Accorsi, Nicola Armaroli,* Henk J. Bolink, Enrique Ortí,* Rosario Scopelliti, Md. Khaja Nazeeruddin, and Etienne Baranoff*

The photophysical behavior of bis-cyclometalated iridium complexes with pyridine–carbene (N^C:) and bis-carbene (:C^C:) ancillary ligands is compared. The use of N^C: ancillary ligands results in thermally accessible low-lying triplet metal-centered (^{3}MC) states and leads to a significant decrease of the photoluminescence quantum yield (Φ_{PL}) in solution, from 30% to 1%, when compared to the :C^C: ancillary ligand. On the contrary, all of the investigated complexes are bright emitters (Φ_{PL} 30–60%) in the solid state (1% poly(methyl methacrylate) matrix) both at room temperature and at 77 K.

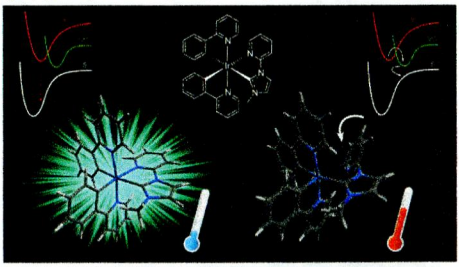

10306 Ⓢ dx.doi.org/10.1021/ic400627c

Easy Synthesis of High-Purity $BiFeO_3$ Nanoparticles: New Insights Derived from the Structural, Optical, and Magnetic Characterization

José Luis Ortiz-Quiñonez, David Díaz,* Inti Zumeta-Dubé, Humberto Arriola-Santamaría, Israel Betancourt, Patricia Santiago-Jacinto, and Noel Nava-Etzana

This graphic represents the two synthesis pathways followed to obtain multiferroic $BiFeO_3$ nanoparticles (NPs). Using tartaric acid, two byproducts, $Bi_2Fe_4O_9$ (5 nm) and β-Bi_2O_3, were formed. $Bi_2Fe_4O_9$ was identified by HRTEM, and a structural instability induced by the electron beam from the microscope is shown. These $BiFeO_3$ NPs showed ferromagnetic behavior. When glycine was used, an intermediate was formed and, then, $BiFeO_3$ NPs without byproducts. The hexagonal cell depicts the octahedral around the Fe cations.

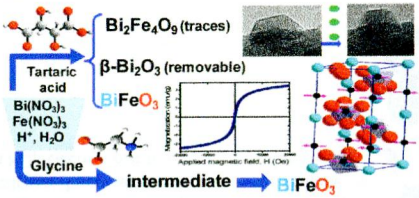

10318 Ⓢ dx.doi.org/10.1021/ic400678u

Hydration Properties and Ionic Radii of Actinide(III) Ions in Aqueous Solution

Paola D'Angelo,* Fausto Martelli, Riccardo Spezia, Adriano Filipponi, and Melissa A. Denecke

Ionic radii in aqueous solution have been derived for actinide(III) cations starting from a very accurate experimental determination of the ion–water distances obtained from extended X-ray absorption fine structure (EXAFS) data in combination with molecular dynamics results. A close similarity between actinide and lanthanide ions has been found.

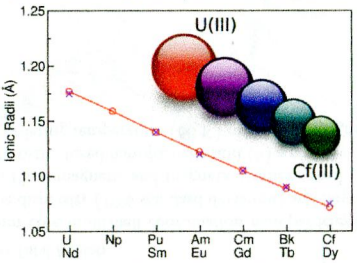

10325 S dx.doi.org/10.1021/ic400767u

Development of a Ruthenium(II) Complex-Based Luminescent Probe for Hypochlorous Acid in Living Cells

Run Zhang, Zhiqiang Ye,* Bo Song, Zhichao Dai, Xin An, and Jingli Yuan*

A unique ruthenium(II) complex, $[Ru(bpy)_2(DNPS\text{-}bpy)](PF_6)_2$ (bpy: 2,2′-bipyridine, DNPS-bpy: 4-(2,4-dinitrophenylthio)methylene-4′-methyl-2,2′-bipyridine), has been designed and synthesized as a highly sensitive and selective luminescence probe for the recognition and detection of hypochlorous acid (HOCl) in living cell samples. The probe can rapidly and specifically react with HOCl to afford a highly luminescent bipyridine-Ru(II) complex derivative, $[Ru(bpy)_2(COOH\text{-}bpy)](PF_6)_2$ (COOH-bpy: 4′-methyl-2,2′-bipyridyl-4-carboxylic acid), accompanied by the remarkable luminescence enhancement.

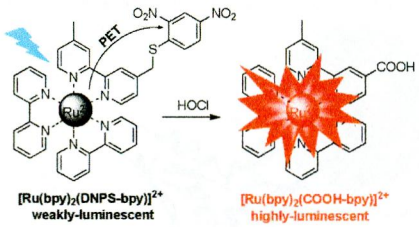

10332 S dx.doi.org/10.1021/ic400955c

Tuning Spin–Spin Coupling in Quinonoid-Bridged Dicopper(II) Complexes through Rational Bridge Variation

David Schweinfurth, Marat M. Khusniyarov,* Denis Bubrin, Stephan Hohloch, Cheng-Yong Su, and Biprajit Sarkar*

A large influence on the spin–spin coupling in dicopper(II) complexes is seen to result on making a simple [O] for [NR] substitution in the quinonoid bridging ligand. The spin density on the coordination atoms of the bridge, as well as the exchange pathway, is seen to drastically change on changing the bridge. DFT calculations have been used to elucidate the mechanism of exchange coupling.

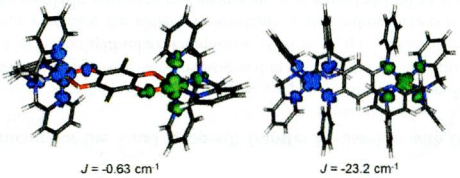

10340 S dx.doi.org/10.1021/ic401033u

Tunable Blue-Green-Emitting $Ba_3LaNa(PO_4)_3F:Eu^{2+},Tb^{3+}$ Phosphor with Energy Transfer for Near-UV White LEDs

Mengmeng Jiao, Ning Guo, Wei Lü, Yongchao Jia, Wenzhen Lv, Qi Zhao, Baiqi Shao, and Hongpeng You*

A novel color tunable $Ba_3LaNa(PO_4)_3F:Eu^{2+},Tb^{3+}$ phosphor has been synthesized by high temperature solid state reaction. The obtained samples have strong absorption in the n-UV range, which matches well with the commercial n-UV LED chips. By tuning the relative content of the doped ions, tunable blue-green emission can be obtained by the irradiation at 400 nm. The prepared phosphor may have potential application in n-UV white LEDs

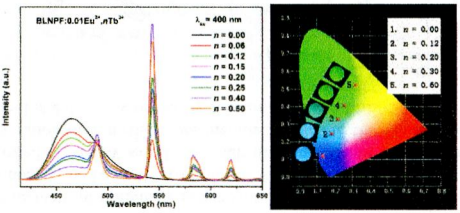

10347 Ⓢ dx.doi.org/10.1021/ic401037x

Predicting the Stability Constants of Metal-Ion Complexes from First Principles

Ondrej Gutten and Lubomír Rulíšek*

Predicting the stability constants of transition-metal-ion complexes in solution represents a challenge for which contemporary computational chemistry may not yet be able to provide final answers. However, careful use of modern computational methods in combination with advanced solvation models, such as COSMO-RS, can at least provide quantitative estimates of the *relative* affinities for a series of metal ions and a number of insights into this intriguing topic.

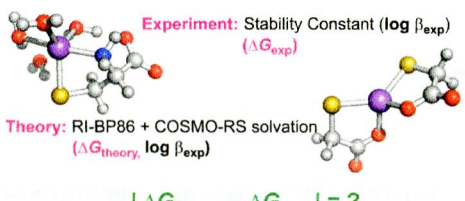

10356 Ⓢ dx.doi.org/10.1021/ic401060k

Supramolecular β-Cyclodextrin Adducts of Boron-Rich DNA Metallointercalators Containing Dicarba-*closo*-dodecaborane(12)

H. Y. Vincent Ching, Ronald J. Clarke, and Louis M. Rendina*

A chiral, isomeric series of novel boron-rich Pt^{II} metallointercalators containing two *N*-donor carboranylpyridyl ligands were prepared and fully characterized, and the corresponding water-soluble supramolecular 2:1 host–guest β-cyclodextrin (β-CD) adducts ($[PtL_2(phen)\cdot 2\beta\text{-CD}](NO_3)_2$) were also prepared and fully characterized. The interaction of the novel supramolecular adducts with calf thymus DNA was investigated by means of comprehensive linear dichroism, ultraviolet-visible spectroscopy, thermal denaturation, and isothermal titration calorimetry experiments.

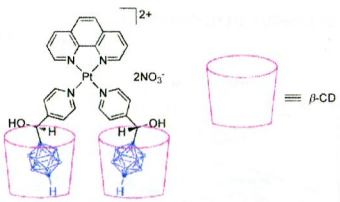

10368 Ⓢ dx.doi.org/10.1021/ic401092j

A Porous Metal–Organic Framework Constructed from Carboxylate–Pyrazolate Shared Heptanuclear Zinc Clusters: Synthesis, Gas Adsorption, and Guest-Dependent Luminescent Properties

Qingshu Zheng, Feilong Yang, Mingli Deng, Yun Ling,* Xiaofeng Liu, Zhenxia Chen, Yunhua Wang, Linhong Weng, and Yaming Zhou*

Solvothermal reaction of 4,4′-biphenyldicarboxylic acid (H_2bpdc), 3,5-dimethyl-4-(4′-pyridyl)pyrazole (Hdmpp) and zinc salt affords to the formation of a porous structure of $[Zn_7O_2(bpdc)_4(dmpp)_2]\cdot 6DEF\cdot 10H_2O$ (MAC-7), which is built of a novel 12-bridged carboxylate-pyrazolate shared heptanuclear zinc cluster. It can be used as a candidate for sensing nitrobenzene molecule over toluene, *p*-xylene, mesitylene, and cyclohexane by luminescent quenching.

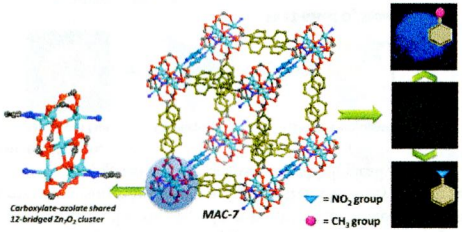

10375 Ⓢ dx.doi.org/10.1021/ic401104m

Synthesis and Characterization of Nonsubstituted and Substituted Proton-Conducting $La_{6-x}WO_{12-y}$

Janka Seeger,* Mariya E. Ivanova, Wilhelm A. Meulenberg, Doris Sebold, Detlev Stöver, Tobias Scherb, Gerhard Schumacher, Sonia Escolástico, Cecilia Solís, and José M. Serra

For increasing the electrical conductivity of nominally nonsubstituted lanthanum tungstate $La_{6-x}WO_{12-y}$ (with $y = 1.5x + \delta$ and $x = 0.5-0.8$) partial substitution of the La or W position was implemented. Remarkable improvement was achieved when 20 mol % Re or Mo was substituted on the W site. La-site substitution was not that effective. Nonsubstituted $La_{6-x}WO_{12-y}$ compounds with different La/W ratios were furthermore manufactured, and the temperature dependence of single-phase formation was studied. Compound stability was tested by Raman, XRD, and SEM.

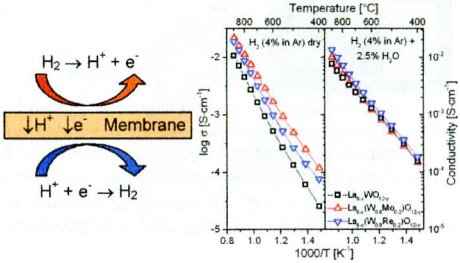

10387 Ⓢ dx.doi.org/10.1021/ic401106z

Investigating the Electronic Structure of the Atox1 Copper(I) Transfer Mechanism with Density Functional Theory

Amanda L. Pitts and Michael B. Hall*

The electronic structure of the Cu(I)−Cys interactions during the copper transfer between Atox1 and a metal binding domain on the ATP7A or ATP7B protein was computationally investigated in this work. Density functional theory was used to explore the electronic struture of three Cu(I) methylthiolate complexes, $[Cu(SCH_3)_2]^{-1}$, $[Cu(SCH_3)_3]^{-2}$, $[Cu(SCH_3)_4]^{-3}$, and a model transfer mechanism to fully elucidate the electronic structure and bonding between Cu(I) and thiolate species. The electronic structure was found to similarly influence the geometry of the methylthiolate species and the model transfer mechanism. These conclusions predict that the Cu(I)−Cys electronic structure in concert with the van der Waals and electrostatic interactions in the full protein environment determine the configuration of the donor−acceptor adduct during Cu(I) transfer.

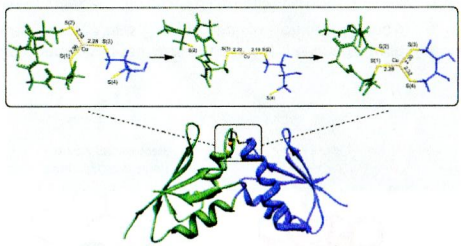

10394 Ⓢ dx.doi.org/10.1021/ic4011168

Two-Photon Oxygen Sensing with Quantum Dot-Porphyrin Conjugates

Christopher M. Lemon, Elizabeth Karnas, Moungi G. Bawendi,* and Daniel G. Nocera*

Nanosized chemosensors have been developed to probe oxygen concentrations in biological systems that consist of palladium(II) porphyrins with *meso*-pyridyl substituents, which bind to the surface of CdSe quantum dots (QDs). Spectral overlap of QD emission and porphyrin absorption results in high FRET efficiency, which serves as the mechanism for signal transduction in these constructs. These conjugates are responsive in the biologically relevant O_2 pressure range of 0−160 Torr under both one- and two-photon excitation.

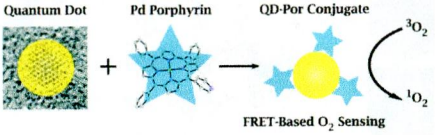

10407 dx.doi.org/10.1021/ic401854r

Triple-Layered Perovskite Niobates $CaRNb_3O_{10}$ (R = La, Sm, Eu, Gd, Dy, Er, Yb, or Y): New Self-Activated Oxides

Lin Qin, Donglei Wei, Yanlin Huang,* Sun Il Kim, Young Moon Yu, and Hyo Jin Seo*

The layered perovskite-like $CaRNb_3O_{10}$ (R = La, Sm, Eu, Gd, Dy, Er, Yb, Y) presents tunable colors under UV light with different R ions in the host. $CaRNb_3O_{10}$ (R = La, Gd, Yb, Y) show the CT transition luminescence related to the NbO_6 octahedra. $CaRNb_3O_{10}$ (R = Sm, Er, Dy, Eu) show emission lines from f→f transitions which overlapped with the broad luminescence band from NbO_6 groups.

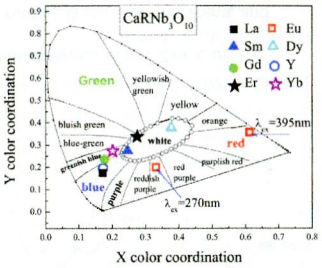

10414 Ⓢ dx.doi.org/10.1021/ic4011955

Mn_8 Cluster with Ferrocene-1,1′-Dicarboxylate Ligation: Single-Molecule Magnetism with Multiple External Redox Centers

Antonio Masello, Khalil A. Abboud, Wolfgang Wernsdorfer, and George Christou*

The use of ferrocene-1,1′-dicarboxylic acid ($fdcH_2$) in Mn cluster chemistry has given a new $Mn^{III}_4Mn^{II}_4$ cluster that was obtained in two forms: $[Mn_8O_4(fdc)_6(DMF)_2(H_2O)_2]$ (**1**) and $[Mn_8O_4(fdc)_6(DMF)_4]$ (**2**). These are structurally similar but nevertheless exhibit significant differences in metric parameters that lead to different magnetic properties, with ground states of $S = 5$ and $S = 2$ for **1** and **2**, respectively. Magnetization hysteresis loops were observed for single crystals of **1**·4DMF·$4H_2O$, confirming it to be a new single-molecule magnet.

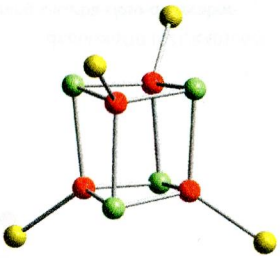

10424 S dx.doi.org/10.1021/ic401253q

Pairwise Assembly of Organopalladium(II) Units with Cyanurato(3−) and Trithiocyanurato(3−) Ligands: Formation of Chiral Pd_{12}, Pd_{10}, and Pd_9 Cage-Molecules

Claire A. Murray, Christine J. Cardin, Barnaby W. Greenland, Andrew Swift, and Howard M. Colquhoun*

The *o*-palladated, chloro-bridged dimers $[Pd\{2\text{-phenylpyridine}(-H)\}\text{-}\mu\text{-}Cl]_2$ and $[Pd\{N,N\text{-dimethylbenzylamine}(-H)\}\text{-}\mu\text{-}Cl]_2$ react with cyanuric acid in the presence of base to afford closed, chiral cage-molecules (point group *T*) in which 12 organo-Pd(II) centers located about the vertices of an octahedron are linked by four tetrahedrally arranged cyanurato(3−) ligands. Incomplete (Pd_{10}) cages have also been isolated. Reaction of $[Pd\{2\text{-phenylpyridine}(-H)\}\text{-}\mu\text{-}Cl]_2$ with trithiocyanuric acid gives a cage-complex comprising only nine organopalladium centers and three thiocyanurato(3−) ligands.

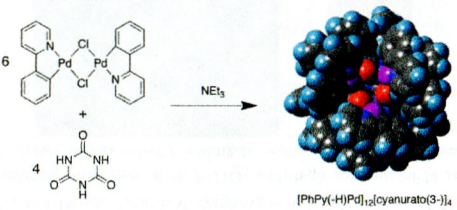

10431 S dx.doi.org/10.1021/ic401261z

Redox Properties of a Mononuclear Copper(II)-Superoxide Complex

Tetsuro Tano, Yuri Okubo, Atsushi Kunishita, Minoru Kubo, Hideki Sugimoto, Nobutaka Fujieda, Takashi Ogura, and Shinobu Itoh*

Reactions of a mononuclear copper(II)-superoxide complex having a distorted tetrahedral geometry toward several types of external substrates such as one-electron reductants, hydrogen-atom donors, and oxygen-atom acceptors have been examined in detail to explore the intrinsic reactivity of the superoxide complex and the generated copper products.

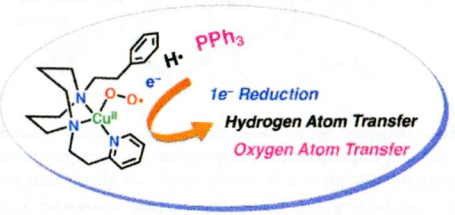

10438 dx.doi.org/10.1021/ic401274p

Rich Crystal Chemistry and Magnetism of "114" Stoichiometric $LnBaFe_4O_{7.0}$ Ferrites

V. Duffort, V. Caignaert,* V. Pralong, A. Cervellino, D. Sheptyakov, and B. Raveau

Stoichiometric $LnBaFe_4O_{7.0}$ oxides with Ln = Dy to Lu have been synthesized and protected in order to prevent oxidation. At room temperature these compounds are tetragonal ($I\bar{4}$), and at higher temperature (T > 580 K) they exhibit cubic symmetry ($F\bar{4}3m$). Moreover, the low-temperature structures of these oxides are dependent on the nature of the Ln^{3+} cation. Neutron diffraction patterns evidence long-range magnetic ordering only for the most distorted structures (Ln = Dy and Ho). The behavior of these "114" iron oxides is compared to the cobalt family, showing in both cases a striking underbonding of barium.

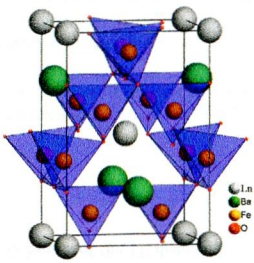

10449 Ⓢ dx.doi.org/10.1021/ic401289k

Facile η^5–η^1 Ring Slippage of the Cycloolefin Ligands in Osmocene and Bis(η^5-indenyl)ruthenium(II)

Wai-Man Cheung, Enrique Kwan Huang, Jun Zhu,* Xiao-Yi Yi, Herman H. Y. Sung, Ian D. Williams, and Wa-Hung Leung*

Reactions of $[OsCp_2]$ (Cp = η^5-C_5H_5) and $[Ru(\eta^5\text{-ind})_2]$ (ind = indenyl) with the ruthenium(VI) nitride $[Ru(L_{OEt})(N)Cl_2]$ ($L_{OEt}^- = [CoCp\{P(O)(OEt)_2\}_3]^-$) result in η^5–η^1 slippage of the cycloolefin ligands and formation of the trinuclear nitrido complexes $[Cp(\eta^1\text{-}C_5H_5)Os(NRuL_{OEt}Cl_2)_2]$ and $[(\eta^5\text{-ind})(\eta^1\text{-ind})Ru\text{-}(NRuL_{OEt}Cl_2)_2]$, respectively.

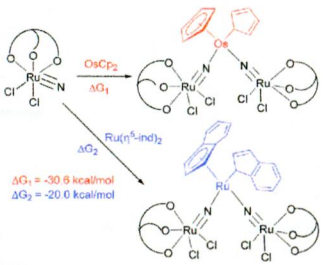

10456 Ⓢ dx.doi.org/10.1021/ic401280e

Marinite $Li_2M(SO_4)_2$ (M = Co, Fe, Mn) and $Li_1Fe(SO_4)_2$: Model Compounds for Super-Super-Exchange Magnetic Interactions

Marine Reynaud, Gwenaëlle Rousse,* Jean-Noël Chotard, Juan Rodríguez-Carvajal, and Jean-Marie Tarascon

A new manganese-based member of the marinite $(Li_2M(SO_4)_2)$ series has been prepared, and the structure of the delithiated iron analogue $Li_1Fe(SO_4)_2$ has been solved. The four compounds $Li_2M^{II}(SO_4)_2$ (M = Co, Fe, Mn) and $Li_1Fe^{III}(SO_4)_2$ are antiferromagnetic, and neutron powder diffraction was used to determine their ground-state magnetic structures. Analyses of the super-super-exchange interactions are in agreement with Goodenough–Kanamori–Anderson rules.

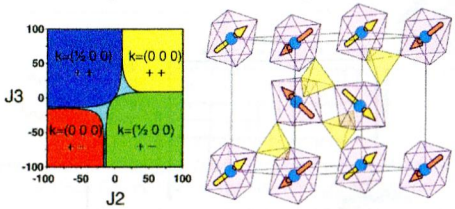

10467 Ⓢ dx.doi.org/10.1021/ic4013558

Synthesis and Ligand Non-Innocence of Thiolate-Ligated (N_4S) Iron(II) and Nickel(II) Bis(imino)pyridine Complexes

Leland R. Widger, Yunbo Jiang, Maxime A. Siegler, Devesh Kumar, Reza Latifi, Sam P. de Visser,* Guy N. L. Jameson,* and David P. Goldberg*

A series of iron(II) and nickel(II) thiolate-ligated, bis(imino)pyridine complexes was prepared with a tetradentate ligand, LN_3S. The data show that these complexes can be reduced by one electron, and LN_3S is non-innocent. The one-electron-reduced $[Fe^{II}(LN_3S)(DMAP]^0$ (**4**) was characterized by X-ray crystallography, UV-vis, EPR, and Mössbauer spectroscopy, as well as DFT calculations. From these data, **4** can best be described as an intermediate-spin iron(II) ($S = 1$) center antiferromagnetically coupled to a ligand-based radical.

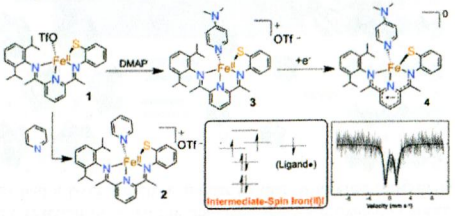

10481 dx.doi.org/10.1021/ic401385f

Influence of Lattice Interactions on the Jahn–Teller Distortion of the $[Cu(H_2O)_6]^{2+}$ Ion: Dependence of the Crystal Structure of $K_{2x}Rb_{2-2x}[Cu(H_2O)_6](SeO_4)_2$ upon the K/Rb Ratio

Charles J. Simmons,* Horst Stratemeier, Michael A. Hitchman, and Mark J. Riley

For the mixed-cation salts $K_{2x}Rb_{2-2x}[Cu(H_2O)_6](SeO_4)_2$, a different crystal form (form **A**) is observed for a low proportion of potassium compared with a high proportion (form **B**), with the long and intermediate Cu–O bonds of the JT distorted $[Cu(H_2O)_6]^{2+}$ ion occurring with a different pair of water molecules in the two forms.

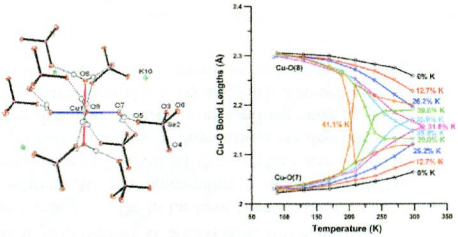

10500 dx.doi.org/10.1021/ic401410g

d→f Energy Transfer in Ir(III)/Eu(III) Dyads: Use of a Naphthyl Spacer as a Spatial and Energetic "Stepping Stone"

Daniel Sykes, Simon C. Parker, Igor V. Sazanovich, Andrew Stephenson, Julia A. Weinstein,* and Michael D. Ward*

If the Ir-based ^{3}MLCT/^{3}LC excited state is high enough in energy, in Ir–naphthyl–Eu triads the triplet excited state of the naphthyl group (^{3}nap) acts as a spatial and energetic intermediate for two-step Ir→^{3}nap and then ^{3}nap→Eu energy-transfer; the grow-in and decay of the ^{3}nap state as it receives and then passes on the excitation energy can be followed by transient absorption spectroscopy.

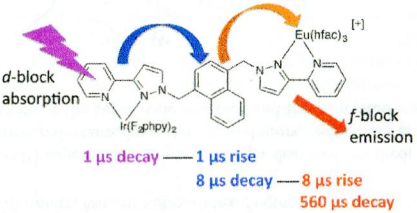

10512 dx.doi.org/10.1021/ic401426q

Synthesis, Characterization, Photocatalysis, and Varied Properties of TiO_2 Cosubstituted with Nitrogen and Fluorine

Nitesh Kumar, Urmimala Maitra, Vinay I. Hegde, Umesh V. Waghmare, A. Sundaresan, and C. N. R. Rao*

Structural, electronic, and water-splitting properties of N, F-TiO_2 with high contents of N and F are described. N, F-cosubstituted TiO_2 exhibits good photocatalytic activity leading to significant H_2 evolution under visible light irradiation.

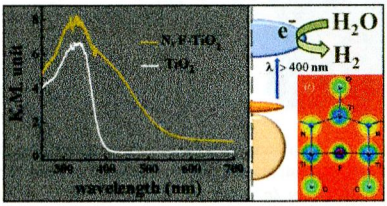

10520 Ⓢ dx.doi.org/10.1021/ic4014587

Phase Transition between Layered Tungstates and Polyoxotungstates in Aqueous Solutions

Takayuki Ban,* Toshihiro Ito, and Yutaka Ohya

The dissolution and precipitation of tetramethylammonium tungstate occurred reversibly in aqueous solutions. When polyoxotungstate was dissolved, the reaction between the dissolved species provided colloidal-layered tungstate nanocrystals. The layered tungstate nanocrystals had a layer structure similar to that of layered tungstic acid $H_2WO_4 \cdot H_2O$.

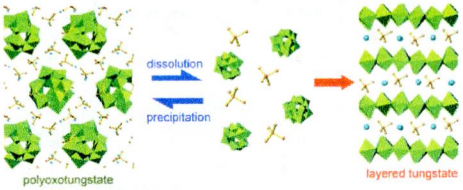

10525 dx.doi.org/10.1021/ic401480b

In Situ Neutron Powder Diffraction of the Formation of $SrGa_2D_2$, and Hydrogenation Behavior of $YbGa_2$ and $EuGa_2$

Patrick Wenderoth and Holger Kohlmann*

With the help of in situ neutron powder diffraction, the behavior of $SrGa_2$ during the formation of its deuteride $SrGa_2D_2$ is shown. Additionally, results of hydrogenation experiments on the structurally related compounds $EuGa_2$ and $YbGa_2$ are presented, and the first refined crystal structure data of $YbGa_6$ are given.

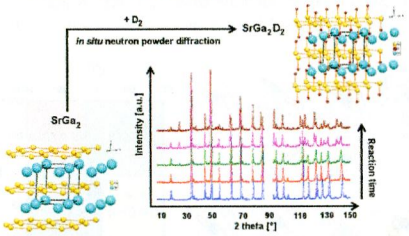

10532 Ⓢ dx.doi.org/10.1021/ic401499j

Speciation of Platinum(IV) in Nitric Acid Solutions

Danila Vasilchenko,* Sergey Tkachev, Iraida Baidina, and Sergey Korenev

New data regarding the speciation of Pt(IV) in concentrated nitric acid (6–15.8M) solutions obtained by means of ^{195}Pt NMR and Raman spectroscopy, as well as crystal structures of new $[Pt(NO_3)_6]^{2-}$ and $[Pt_2(\mu\text{-}OH)_2(NO_3)_8]^{2-}$ complexes, are reported.

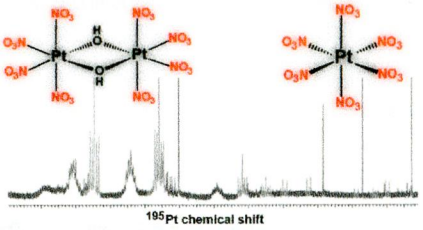

10542 dx.doi.org/10.1021/ic4015256

Ferroelectric Mesocrystals of Bismuth Sodium Titanate: Formation Mechanism, Nanostructure, and Application to Piezoelectric Materials

Dengwei Hu, Xingang Kong, Kotaro Mori, Yasuhiro Tanaka, Kazunari Shinagawa, and Qi Feng*

Ferroelectric mesocrystals of $Bi_{0.5}Na_{0.5}TiO_3$ (BNT) with [100]-crystal-axis orientation were successfully prepared using a topotactic structural transformation process from a layered titanate $H_{1.07}Ti_{1.73}O_4{\cdot}nH_2O$ (HTO). The formation reactions of BNT mesocrystals in HTO–Bi_2O_3–Na_2CO_3 and HTO–TiO_2–Bi_2O_3–Na_2CO_3 reaction systems and their nanostructures were studied by XRD, FE-SEM, TEM, SAED, and EDS, and the reaction mechanisms were given.

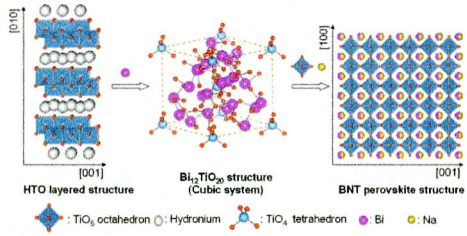

10552 dx.doi.org/10.1021/ic401532j

Uranium(III) Complexes with Bulky Aryloxide Ligands Featuring Metal–Arene Interactions and Their Reactivity Toward Nitrous Oxide

Sebastian M. Franke, Ba L. Tran, Frank W. Heinemann, Wolfgang Hieringer, Daniel J. Mindiola,* and Karsten Meyer*

We report the synthesis and use of an easy-to-prepare, bulky, and robust aryloxide ligand starting from inexpensive precursor materials. Based on this aryloxide ligand, two reactive, coordinatively unsaturated U(III) complexes were prepared that are masked by a metal–arene interaction via δ-backbonding. Depending on solvent and uranium starting material, both a THF-bound and Lewis-base-free U(III) precursor can easily be prepared on the multigram scale.

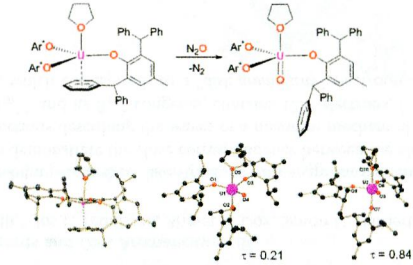

10559 dx.doi.org/10.1021/ic401540s

Intramolecular d^{10}–d^{10} Interactions in a $Ni_6C(CO)_9(AuPPh_3)_4$ Bimetallic Nickel–Gold Carbide Carbonyl Cluster

Iacopo Ciabatti, Cristina Femoni, Maria Carmela Iapalucci, Andrea Ienco, Giuliano Longoni, Gabriele Manca, and Stefano Zacchini*

The $Ni_6C(CO)_9(AuPPh_3)_4$ bimetallic carbide carbonyl cluster was synthesized and its structure elucidated by means of X-ray crystallography and density functional theory calculations, disclosing the presence of weak intramolecular Au···Au d^{10}–d^{10} interactions.

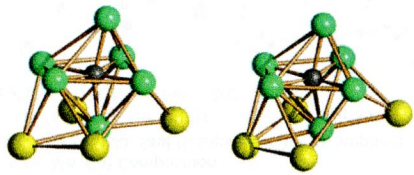

10566 Ⓢ dx.doi.org/10.1021/ic4015465

Three New Mixed-Alkali- and Alkaline-Earth-Metal Borates: From 1D Chain to 2D Layer to 3D Framework

Han-Qing Wu, Ping Ju, Huan He, Bai-Feng Yang, and Guo-Yu Yang*

Three novel mixed-metal borates, $K_4Ba_2[B_{14}O_{20}(OH)_{10}]\cdot 3H_2O$ (**1**), $LiSr_2[B_{10}O_{16}(OH)_3]$ (**2**), and $LiBa[B_9O_{15}]$ (**3**), made under hydro(solvo)thermal conditions, contain different structural building units (SBUs), $B_{14}O_{21}(OH)_{10}$, $B_{10}O_{19}(OH)_3$, and B_3O_7, resulting in different dimensions from 1D chain to 2D layer to 3D framework that depend on the numbers of hydroxyls in the SBUs for **1**−**3**, respectively.

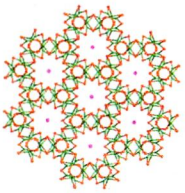

10571 dx.doi.org/10.1021/ic401548a

Topochemical Cross-Linking of the $[Hf_2N_2]$ Layers with Sulfur in α-HfNBr

Shuai Zhang, Mayumi Yoshikawa, Kei Inumaru, and Shoji Yamanaka*

The α-type nitride layers $[Hf_2N_2]$ of α-HfNBr are topochemically cross-linked with sulfur atoms by the reaction with Na_2S.

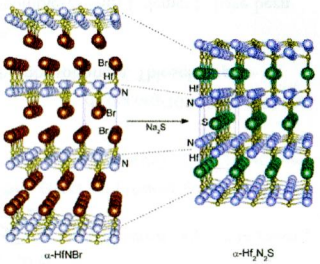

10576 Ⓢ dx.doi.org/10.1021/ic401563f

Self-Organization of Zr(IV) Porphyrinoids on Graphene Oxide Surfaces by Axial Metal Coordination

Matthew Jurow, Viacheslav Manichev, Cesar Pabon, Brian Hageman, Yuliya Matolina, and Charles Michael Drain*

A transmission electron microscope image of a graphene oxide flake functionalized with Zr(IV)phthalocyanine (structure inset). The increased chromophore binding visible along the flake edges is mediated by coordination of the carboxylic acid groups on the graphene oxide to the protruding oxophilic 8-coordinate metal ion.

10583 S dx.doi.org/10.1021/ic401558f

First Row Transition Metal(II) Thiocyanate Complexes, and Formation of 1-, 2-, and 3-Dimensional Extended Network Structures of $M(NCS)_2(Solvent)_2$ (M = Cr, Mn, Co) Composition

Endrit Shurdha, Curtis E. Moore, Arnold L. Rheingold, Saul H. Lapidus, Peter W. Stephens, Atta M. Arif, and Joel S. Miller*

$M(NCS)_2(Sol)_2$ are shown to form 1-D (M = Co; Sol = THF), 2-D (M = Mn; Sol = MeCN), and 3-D (M = Cr; Sol = MeCN) extended structures while $Fe^{II}(NCS)_2TCNQ$ forms a 2-D structure

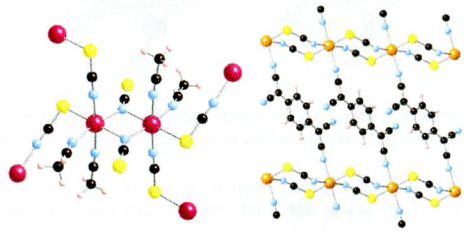

10595 S dx.doi.org/10.1021/ic401596s

Particle on a Boron Disk: Ring Currents and Disk Aromaticity in B_{20}^{2-}

Truong Ba Tai, Remco W. A. Havenith,* Jos L. Teunissen, Ahmet R. Dok, Simon D. Hallaert, Minh Tho Nguyen,* and Arnout Ceulemans*

The B_{20}^{2-} cluster is predicted to exhibit a planar sheet-like structure with a circular circumference. Orbital plots and energy correlations demonstrate the close correspondence between the electronic structure of B_{20}^{2-} and the Bessel functions describing the waves of a quantum mechanical particle confined to a disk. The π-band of B_{20}^{2-}, and its B_{19}^{-} congener, contains 12 π-electrons, forming a $(1\sigma)^2(1\pi)^4(1\delta)^4(2\sigma)^2$ configuration, which corresponds to a "*disk aromaticity*" electron count.

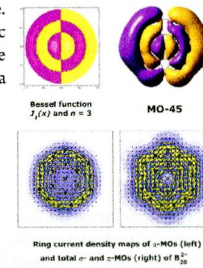

10601 S dx.doi.org/10.1021/ic401626e

N-Benzyl Substituted N-Heterocyclic Carbene Complexes of Iridium(I): Assessment in Transfer Hydrogenation Catalyst

Süleyman Gülcemal,* Aytaç Gürhan Gökçe, and Bekir Çetinkaya

Three new iridium(I)-NHC complexes have been synthesized and found to be highly active catalysts for transfer hydrogenation reaction of various ketones and imines.

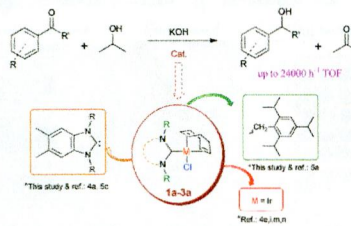

10610 S dx.doi.org/10.1021/ic401633c

Solid Solutions of Pauli-Paramagnetic $CaCu_3V_4O_{12}$ and Antiferromagnetic $CaMn_3V_4O_{12}$

Shoubao Zhang, Takashi Saito, Wei-Tin Chen, Masaichiro Mizumaki, and Yuichi Shimakawa*

Solid solutions of Pauli-paramagnetic $CaCu_3V_4O_{12}$ and antiferromagnetic $CaMn_3V_4O_{12}$ were prepared, and the changes in the crystal and electronic structures and magnetic and transport properties were clarified.

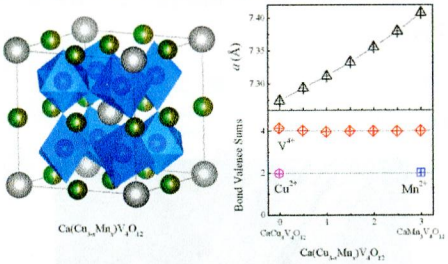

10615 S dx.doi.org/10.1021/ic4016383

A Ru(II) Bis-terpyridine-like Complex that Catalyzes Water Oxidation: The Influence of Steric Strain

Nattawut Kaveevivitchai, Lars Kohler, Ruifa Zong, Maya El Ojaimi, Nirja Mehta, and Randolph P. Thummel*

The reactivity of certain Ru(II) bis-terpyridine-type complexes toward water oxidation is strongly influenced by steric strain effects leading to the pentagonal bipyramidal seven-coordinate intermediate: angle strain is required in the equatorial plane as well as a linear arrangement of the axial ligands.

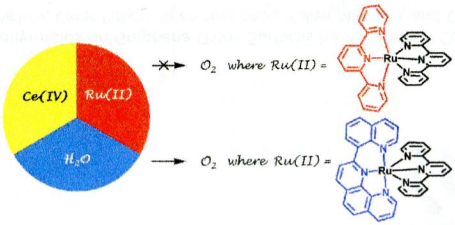

10623 S dx.doi.org/10.1021/ic401642a

Systematic Investigation of Thorium(IV)– and Uranium(IV)–Ligand Bonding in Dithiophosphonate, Thioselenophosphinate, and Diselenophosphonate Complexes

Andrew C. Behrle, Charles L. Barnes, Nikolas Kaltsoyannis,* and Justin R. Walensky*

The first actinide dithio- and diselenophosphonate as well as thioselenophosphinate complexes with f elements have been characterized, and their bonding has been analyzed through density functional theory calculations. Results reveal increased covalent bonding character in actinide–selenium bonds than those with sulfur.

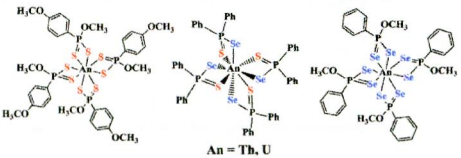

10632 S dx.doi.org/10.1021/ic401666m

Design Criteria for Polyazine Extractants To Separate An^{III} from Ln^{III}

Charles de Sahb, Lori A. Watson, Janos Nadas, and Benjamin P. Hay*

This theoretical study evaluates the fundamental properties of azine donors and uses this information to identify azine compositions in the TERPY architecture that yield optimal extractants for actinide/lanthanide partitioning.

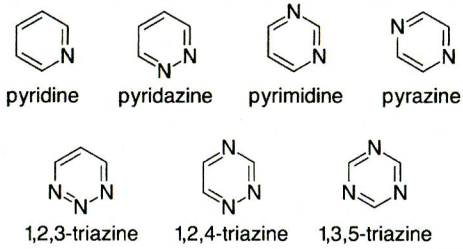

10643 S dx.doi.org/10.1021/ic401684u

Dicopper Double-Strand Helicates Held Together by Additional $\pi-\pi$ Interactions

Massimo Boiocchi, Valentina Brega, Carlo Ciarrocchi, Luigi Fabbrizzi,* and Piersandro Pallavicini

The bis-bidentate ligand L–L forms with two Cu^{I} ions a double strand helicate complex, made especially stable by the presence of four definite interstrand $\pi-\pi$ interactions. The $[Cu^{I}_2(L-L)_2]^{2+}$ complex in MeCN undergoes two one-electron oxidation processes to the dicopper(II) derivative, separated by 260 mV.

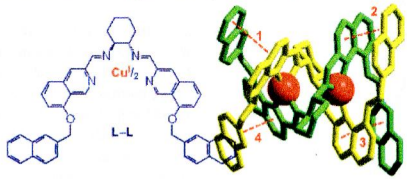

10653 dx.doi.org/10.1021/ic401704r

Electronic Spectra of *N*-Heterocyclic Pentacyanoferrate(II) Complexes in Different Solvents, Studied by Multiconfigurational Perturbation Theory

André Luiz Barboza Formiga,* Steven Vancoillie, and Kristine Pierloot*

Ligand-field and charge-transfer spectra of *N*-heterocyclic pentacyanoferrate(II) complexes were calculated by means of multiconfigurational perturbation theory including implicit and explicit solvation. The CASPT2 approach is capable of predicting experimental excitation energies and intensities.

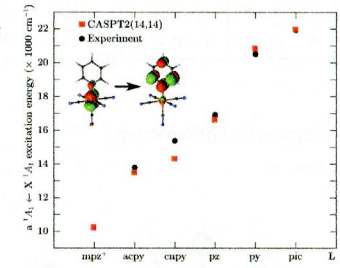

10664 S dx.doi.org/10.1021/ic401698a

Neutral Six-Coordinate and Cationic Five-Coordinate Silicon(IV) Complexes with Two Bidentate Monoanionic *N,S*-Pyridine-2-thiolato(−) Ligands

Johannes A. Baus, Christian Burschka, Rüdiger Bertermann, Célia Fonseca Guerra, F. Matthias Bickelhaupt,* and Reinhold Tacke*

A series of neutral six-coordinate and cationic five-coordinate silicon(IV) complexes (**4**−**12**) with two bidentate monoanionic *N,S*-pyridine-2-thiolato ligands and two (or one, **12**) monodentate ligands R^1 and R^2 was synthesized. Compounds **4**−**12** were characterized by elemental analyses, NMR spectroscopic studies in the solid state and in solution, and crystal structure analyses (except **7**). These structural investigations were performed with a special emphasis on the sophisticated stereochemistry of these compounds. These experimental investigations were complemented by computational studies, including bonding analyses based on relativistic density functional theory.

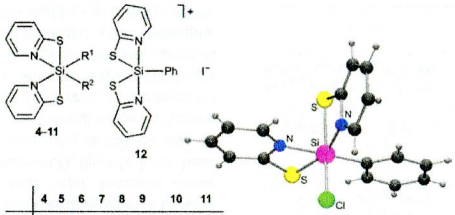

	4	5	6	7	8	9	10	11
R^1	Cl	Ph	Ph	Ph	Ph	Ph	Ph	Me
R^2	Cl	Cl	F	Br	N_3	NCO	NCS	Cl

10677 S dx.doi.org/10.1021/ic401744h

Reaction of 13-Vertex Carborane μ-1,2-$(CH_2)_4$-1,2-$C_2B_{11}H_{11}$ with Nucleophiles: Linkage Effect on Product Formation

Jian Zhang and Zuowei Xie*

The carbon-chain length between two cage carbon atoms has a great influence on the reactivity of 13-vertex carboranes toward nucleophiles, leading to the preparation of carborane derivatives with different cage structures.

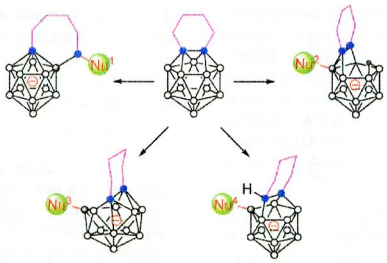

10685 S dx.doi.org/10.1021/ic4018135

New Layered Fluorosulfide $SrFBiS_2$

Hechang Lei, Kefeng Wang, Milinda Abeykoon, Emil S. Bozin, and Cedomir Petrovic*

A new layered BiS_2-based compound, $SrFBiS_2$, has been synthesized that has a similar structure to $LaOBiS_2$. $SrFBiS_2$ is a semiconductor and has a small thermal conductivity and large Seebeck coefficient. $SrFBiS_2$ may be a parent compound of new superconductors.

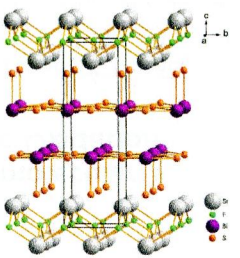

10690 Ⓢ

dx.doi.org/10.1021/ic401844m

Syntheses and Characterizations of Linear Triborazanes

William C. Ewing, Patrick J. Carroll, and Larry G. Sneddon*

A greatly improved method for the synthesis of anionic five-membered, linear aminoborane chains, $[BH_3N(R)HBH_2N(R)HBH_3^-]$, where R = H, Me, and Bz, has been achieved along with conversion of these anions to the first examples of linear triborazanes $BH_3(RNHBH_2)_2N(R)H_2$.

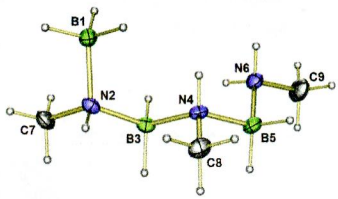

10698 Ⓢ

dx.doi.org/10.1021/ic402041p

Structure and Magnetic Properties of $BiFe_{1-x}Co_xO_3$ and $Bi_{0.9}Sm_{0.1}Fe_{1-x}Co_xO_3$

Makoto Kubota,* Kengo Oka, Hisato Yabuta, Kaoru Miura, and Masaki Azuma

$BiFe_{1-x}Co_xO_3$ and $Bi_{0.9}Sm_{0.1}Fe_{1-x}Co_xO_3$ were synthesized under high pressure. Sm substitution in $BiFe_{1-x}Co_xO_3$ ($x \leq 0.20$) destabilized the ferroelectric $BiFeO_3$-type structure and changed it to an antiferroelectric $PbZrO_3$-type superstructure. Weak ferromagnetism was observed for $BiFe_{1-x}Co_xO_3$ ($x = 0.10$ and 0.20) samples, suggesting the change in the spin structure from a cycloidal one, so this compound is a promising multiferroic material.

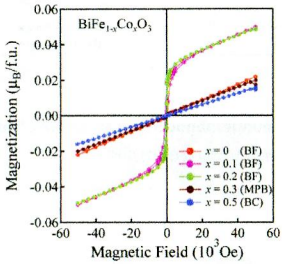

Ⓢ Supporting Information available via online article